A GENERALISED RANDOM ENCOUNTER MODEL FOR ESTIMATING ANIMAL DENSITY WITH REMOTE SENSOR DATA

Running title: A generalised random encounter model for animals.

Word count:

Authors:

Tim C.D. Lucas[1,2,3]†, Elizabeth A. Moorcroft[1,4,5]†, Robin Freeman[5], Marcus J. Rowcliffe[5], Kate E. Jones[2,5]

Addresses:

1 CoMPLEX, University College London, Physics Building, Gower Street, London, WC1E 6BT, UK

2 Centre for Biodiversity and Environment Research, Department of Genetics, Evolution and Environment, University College London, Gower Street, London, WC1E 6BT, UK

3 Department of Statistical Science, University College London, Gower Street, London, WC1E 6BT, UK

4 Department of Computer Science, University College London, Gower Street, London, WC1E 6BT, UK

5 Institute of Zoology, Zoological Society of London, Regents Park, London, NW1 4RY, UK

† First authorship shared.

Corresponding authors:

Kate E. Jones,

Centre for Biodiversity and Environment Research,

Department of Genetics, Evolution and Environment,

University College London,

Gower Street,

London,

WC1E 6BT,

29 UK

30 kate.e.jones@ucl.ac.uk

31

32 Marcus J. Rowcliffe,

33 Institute of Zoology,

34 Zoological Society of London,

35 Regents Park,

36 London,

37 NW1 4RY,

38 UK

39 marcus.rowcliffe@ioz.ac.uk

ABSTRACT

1: Wildlife monitoring technology is advancing rapidly and the use of remote sensors such as camera traps and acoustic detectors is becoming common in both the terrestrial and marine environments. Current methods to estimate abundance or density require individual recognition of animals or knowing the distance of the animal from the sensor, which is often difficult. A method without these requirements, the random encounter model (REM), has been successfully applied to estimate animal densities from count data generated from camera traps. However, count data from acoustic detectors do not fit the assumptions of the REM due to the directionality of animal signals.

2: We developed a generalised REM (gREM), to estimate absolute animal density from count data from both camera traps and acoustic detectors. We derived the gREM for different combinations of sensor detection widths and animal signal widths (a measure of directionality). We tested the accuracy and precision of this model using simulations of different combinations of sensor detection widths and animal signal widths, number of captures, and models of animal movement.

3: We find that the gREM produces accurate estimates of absolute animal density for all combinations of sensor detection widths and animal signal widths. However, larger sensor detection and animal signal widths were found to be more precise. While the model is accurate for all capture efforts tested, the precision of the estimate increases with the number of captures. We found no effect of different animal movement models on the accuracy and precision of the gREM.

4: We conclude that the gREM provides an effective method to estimate absolute animal densities from remote sensor count data over a range of sensor and animal signal widths. The gREM is applicable for count data obtained in both marine and terrestrial environments, visually or acoustically (e.g., big cats, sharks, birds, bats and cetaceans). As sensors such as camera traps and acoustic detectors become more ubiquitous, the gREM will be increasingly useful for monitoring unmarked animal populations across broad spatial, temporal and taxonomic scales.

Keywords. Acoustic detection, camera traps, marine, population monitoring, simulations, terrestrial

INTRODUCTION

Animal population density is one of the fundamental measures in ecology and conservation. The density of a population has important implications for a range of issues such as sensitivity to stochastic fluctuations (Richter-Dyn & Goel, 1972; Wright & Hubbell, 1983) and risk of extinction (Purvis *et al.*, 2000). Monitoring animal population changes in response to anthropogenic pressure is becoming increasingly important as humans rapidly modify habitats and change climates (Everatt *et al.*, 2014). Sensor technology, such as camera traps (Karanth, 1995; Rowcliffe & Carbone, 2008) and acoustic detectors (Clark, 1995; O'Farrell & Gannon, 1999; Acevedo & Villanueva-Rivera, 2006) are becoming increasingly used to monitor changes in animal populations (Rowcliffe & Carbone, 2008; Kessel *et al.*, 2014; Jones *et al.*, 2013), as they are efficient, relativity cheap and non-invasive (Cutler & Swann, 1999), allowing for surveys over large areas and long periods. However, converting sampled count data into estimates of density is problematic as detectability of animals needs to be accounted for (Anderson, 2001).

Existing methods for estimating animal density often require additional information that may not be available. For example, capture-mark-recapture methods (Karanth, 1995; Trolle & Kéry, 2003; Soisalo & Cavalcanti, 2006; Trolle *et al.*, 2007; Borchers *et al.*, 2014) require recognition of individuals, and distance methods (Harris *et al.*, 2013) require an estimation of how far away individuals are from the sensor (Barlow & Taylor, 2005; Marques *et al.*, 2011). The development of the random encounter model (REM) (a modification of a gas model) has enabled animal densities to be estimated from unmarked individuals of a known speed, and with known sensor detection parameters (Rowcliffe *et al.*, 2008). The REM method has been successfully applied to estimate animal densities from camera trap surveys (Manzo *et al.*, 2012; Zero *et al.*, 2013). However, extending the REM method to other types of sensors (e.g., acoustic detectors) is more problematic, because

98   the original derivation assumes a relatively narrow sensor width (up to $\pi/2$ radi-

99   ans) and that the animal is equally detectable irrespective of its heading (Rowcliffe

100 *et al.*, 2008).

101   Whilst these restrictions are not problematic for most camera trap makes (e.g.,

102 Reconyx, Cuddeback), the REM cannot be used to estimate densities from cam-

103 era traps with a wider sensor width (e.g. canopy monitoring with fish eye lenses

104 Brusa & Bunker (2014). Additionally, the REM method is not useful in estimating

105 densities from acoustic survey data as the acoustic detector angles are often wider

106 than $\pi/2$ radians. Acoustic detectors are designed for a range of diverse tasks and

107 environments (Kessel *et al.*, 2014), which will naturally lead to a wide range of sen-

108 sor detection widths and detection distances. In addition to this, calls emitted by

109 many animals are directional (Blumstein *et al.*, 2011) breaking the assumption of

110 the REM method.

111   There has been a sharp rise in interest around passive acoustic detectors in re-

112 cent years, with a 10 fold increase in publications in the decade between 2000 and

113 2010 (Kessel *et al.*, 2014). Acoustic monitoring is being developed to study many

114 aspects of ecology, including the interactions of animals and their environments

115 (Blumstein *et al.*, 2011; Rogers *et al.*, 2013), the presence and relative abundances of

116 species (Marcoux *et al.*, 2011), biodiversity of an area (Depraetere *et al.*, 2012), and

117 monitoring population trends (Jones *et al.*, 2013).

118   Acoustic data suffers from many of the problems associated with data from

119 camera trap surveys in that individuals are often unmarked so capture-mark-

120 recapture methods cannot be used to estimate densities. In some cases the dis-

121 tance between the animal and the sensor is known, for example when an array of

122 sensors and the position of the animal is estimated by triangulation (Lewis *et al.*,

123 2007). In these situations distance-sampling methods can be applied, a method

124 typically used for marine mammals (Rogers *et al.*, 2013). However, in many cases

125 distance estimation is not possible, for example when single sensors are deployed,

126 a situation typical in the majority of terrestrial acoustic surveys (Elphick, 2008;

127 Buckland *et al.*, 2008). In these cases, only relative measures of local abundance

128 can be calculated, and not absolute densities. This means that comparison of

129 populations between species and sites is problematic without assuming equal de-

130 tectability (Hayes, 2000; Schmidt, 2003; Adams *et al.*, 2013). Equal detectability is

131 unlikely because of differences in environmental conditions, sensor type, habitat,

132 and species biology.

133 In this study we create a generalised REM (gREM), as an extension to the cam-

134 era trap model of Rowcliffe *et al.* (2008), to estimate absolute density from count

135 data from acoustic detectors, or camera traps, where the sensor width can vary

136 from 0 to 2π radians, and the signal given from the animal can be directional. We

137 assessed the accuracy and precision of the gREM within a simulated environment,

138 by varying the sensor detection widths, animal signal widths, number of captures

139 and models of animal movement. We use the simulation results to recommend

140 best survey practice for estimating animal densities from remote sensors.

141   METHODS

142 **Analytical Model.** The REM presented by Rowcliffe *et al.* (2008) adapts the gas

143 model to count data collected from camera trap surveys. The REM is derived as-

144 suming a stationary sensor with a detection width less than $\pi/2$ radians. However,

145 in order to apply this approach more generally, and in particular to acoustic de-

146 tectors, we need both to relax the constraint on sensor detection width, and allow

147 for animals with directional signals. Consequently, we derive the gREM for any

148 detection width, θ, between 0 and 2π with a detection distance *r* giving a circular

149 sector within which animals can be captured (the detection zone) (Figure 1). Ad-

150 ditionally, we model the animal as having an associated signal width α between

151 0 and 2π (Figure 1, see Appendix S1 for a list of symbols). We start deriving the

152 gREM with the simplest situation, the gas model where $\theta = 2\pi$ and $\alpha = 2\pi$.

153 *Gas Model.* Following Yapp (1956), we derive the gas model where sensors can

154 capture animals in any direction and animal signals are detectable from any direc-

155 tion ($\theta = 2\pi$ and $\alpha = 2\pi$). We assume that animals are in a homogeneous environ-

156 ment, and move in straight lines of random direction with velocity *v*. We allow

157 that our stationary sensor can capture animals at a detection distance *r* and that if

158 an animal moves within this detection zone they are captured with a probability

159 of one, while animals outside the zone are never captured.

160   In order to derive animal density, we need to consider relative velocity from

161   the reference frame of the animals. Conceptually, this requires us to imagine that

162   all animals are stationary and randomly distributed in space, while the sensor

163   moves with velocity *v*. If we calculate the area covered by the sensor during the

164   survey period, we can estimate the number of animals the sensor should capture.

165   As a circle moving across a plane, the area covered by the sensor per unit time is

166   $2rv$. The number of expected captures, *z*, for a survey period of *t*, with an animal

167   density of *D* is $z = 2rvtD$. To estimate the density, we rearrange to get $D = z/2rvt$.

168   *gREM derivations for different detection and signal widths.* Different combinations of

169   θ and α would be expected to occur (e.g., sensors have different detection widths

170   and animals have different signal widths). For different combinations θ and α, the

171   area covered per unit time is no longer given by $2rv$. Instead of the size of the

172   sensor detection zone having a diameter of $2r$, the size changes with the approach

173   angle between the sensor and the animal. For any given signal width and detec-

174   tor width and depending on the angle that the animal approaches the sensor, the

175   width of the area within which an animal can be detected is called the profile, *p*.

176   The size of the profile (averaged across all approach angles) is defined as the aver-

177   age profile $\bar{p}$. However, different combinations of θ and α need different equations

178   to calculate $\bar{p}$.

179   We have identified the parameter space for the combinations of θ and α for

180   which the derivation of the equations are the same (defined as sub-models in the

181   gREM) (Figure 2). For example, the gas model becomes the simplest gREM sub-

182   model (upper right in Figure 2) and the REM from Rowcliffe *et al.* (2008) is another

183   gREM sub-model where $\theta < \pi/2$ and $\alpha = 2\pi$. We derive one gREM sub-model SE2

184   as an example below, where $2\pi - \alpha/2 < \theta < 2\pi, \ 0 < \alpha < \pi$ (see Appendix S2 for

185   derivations of all gREM sub-models).

186   *Example derivation of SE2.* In order to calculate $\bar{p}$, we have to integrate over the

187   focal angle, x_1 (Figure 3a). This is the angle taken from the centre line of the sensor.

188   Other focal angles are possible (x_2, x_3, x_4) and are used in other gREM sub-models

189   (see Appendix S2). As the size of the profile depends on the approach angle, we

7

present the derivation across all approach angles. When the sensor is directly approaching the animal $x_1 = \pi/2$.

Starting from $x_1 = \pi/2$ until $\theta/2 + \pi/2 - \alpha/2$, the size of the profile is $2r \sin \alpha/2$ (Figure 3b). During this first interval, the size of α limits the width of the profile. When the animal reaches $x_1 = \theta/2 + \pi/2 - \alpha/2$ (Figure 3c), the size of the profile is $r \sin(\alpha/2) + r \cos(x_1 - \theta/2)$ and the size of θ and α both limit the width of the profile (Figure 3c). Finally, at $x_1 = 5\pi/2 - \theta/2 - \alpha/2$ until $x_1 = 3\pi/2$, the width of the profile is again $2r \sin \alpha/2$ (Figure 3d) and the size of α again limits the width of the profile.

The profile width p for π radians of rotation (from directly towards the sensor to directly behind the sensor) is completely characterised by the three intervals (Figure 3b–d). Average profile width $\bar{p}$ is calculated by integrating these profiles over their appropriate intervals of x_1 and dividing by π which gives

$$\bar{p} = \frac{1}{\pi} \left(\int_{\frac{\pi}{2}}^{\frac{\pi}{2}+\frac{\theta}{2}-\frac{\alpha}{2}} 2r \sin \frac{\alpha}{2} \, \mathrm{d}x_1 + \int_{\frac{\pi}{2}+\frac{\theta}{2}-\frac{\alpha}{2}}^{\frac{5\pi}{2}-\frac{\theta}{2}-\frac{\alpha}{2}} r \sin \frac{\alpha}{2} + r \cos\left(x_1 - \frac{\theta}{2}\right) \mathrm{d}x_1 + \int_{\frac{5\pi}{2}-\frac{\theta}{2}-\frac{\alpha}{2}}^{\frac{3\pi}{2}} 2r \sin \frac{\alpha}{2} \, \mathrm{d}x_1 \right)$$

eqn 1

$$= \frac{r}{\pi} \left(\theta \sin \frac{\alpha}{2} - \cos \frac{\alpha}{2} + \cos\left(\frac{\alpha}{2} + \theta\right) \right)$$

eqn 2

We then use this expression to calculate density

$$D = z/vt\bar{p}.$$

eqn 3

Rather than having one equation that describes $\bar{p}$ globally, the gREM must be split into submodels due to discontinuous changes in p as α and β change. These discontinuities can occur for a number of reasons such as a profile switching between being limited by α and θ, the difference between very small profiles and profiles of size zero and the fact that the width of a sector stops increasing once the central angle reaches π radians (i.e., a semi circle is just as wide as a full circle.)

As an example, if α is small, there is an interval between Figure 3c and 3d where the 'blind spot' would prevent animals being detected giving $p = 0$. This would require an extra integral in our equation as simply putting our small value of α into eqn 1 would not give us this integral of $p = 0$.

8

214 gREM submodel specifications were done by hand, and the integration was

215 done using SymPy (SymPy Development Team, 2014) in Python (Appendix S3).

216 The gREM submodels were checked by confirming that: (1) submodels adjacent

217 in parameter space were equal at the boundary between them; (2) submodels that

218 border $\alpha = 0$ had $p = 0$ when $\alpha = 0$; (3) average profile widths $\bar{p}$ were between 0

219 and $2r$ and; (4) each integral, divided by the range of angles that it was integrated

220 over, was between 0 and $2r$. The scripts for these tests are included in Appendix

221 S3 and the R (Team, 2014) implementation of the gREM is given in Appendix S4.

222 **Simulation Model.** We tested the accuracy and precision of the gREM by devel-

223 oping a spatially explicit simulation of the interaction of sensors and animals using

224 different combinations of sensor detection widths, animal signal widths, number

225 of captures, and models of animal movement. 100 simulations were run where

226 each consisted of a 7.5 km by 7.5 km square with periodic boundaries. A station-

227 ary sensor of radius r was set up in the exact centre of each simulation, covering

228 seven sensor detection widths θ, between 0 and 2π ($2/9\pi$, $4/9\pi$, $6/9\pi$, $8/9\pi$, $10/9\pi$,

229 $14/9\pi$, and 2π). Each sensor was set to record continously and to capture ani-

230 mal signals instaneously from emission. Each simulation was populated with a

231 density of 70 animals km^{-2}, calculated from the equation in Damuth (1981) as the

232 expected density of mammals of weighing 1 g. This density therefore represents a

233 reasonable estimate of density of individuals, given that the smallest mammal is

234 around 2 g (Jones *et al.*, 2009). A total of 3937 individuals per simulation were cre-

235 ated which were placed randomly at the start of the simulation. Individuals were

236 assigned 11 signal widths α between 0 and π ($1/11\pi$, $2/11\pi$, $3/11\pi$, $4/11\pi$, $5/11\pi$,

237 $6/11\pi$, $7/11\pi$, $8/11\pi$, $9/11\pi$, $10/11\pi$, π).

238 Each simulation lasted for N steps (14400) of duration T (15 minutes) giving a

239 total duration of 150 days. The individuals moved within each step with a dis-

240 tance d, with an average speed, v. d, was sampled from a normal distribution

241 with mean distance, $\mu_d = vT$, and standard deviation $\sigma_d = vT/10$. An average

242 speed, $v = 40$ km day^{-1}, was chosen as this is the largest day range of terrestrial an-

243 imals (Carbone *et al.*, 2005), and represents the upper limit of realistic speeds. At

244 the end step, individuals were allowed to either remain stationary for a time step

9

245 (with a given probability, S), or change direction (in a uniform distribution with a

246 maximum angle, A) between 0 and π. This resulted in seven different movement

247 models where: (1) simple movement, where S and $A = 0$; (2) stop-start movement,

248 where (i) $S = 0.25$, $A = 0$, (ii) $S = 0.5$, $A = 0$, (iii) $S = 0.75$, $A = 0$; (3) random walk

249 movement, where (i) $S = 0$, $A = \pi/3$, (ii) $S = 0$, $A = 2\pi/3$, iii) $S = 0$, $A = \pi$. Individuals

250 were counted as they moved in and out of the detection zone of the sensor per

251 simulation.

252 We calculated the estimated animal density from the gREM by asumming the

253 number of captures per simulation and inputting these values into the correct

254 gREM submodel. gREM accuracy was determined by comparing the density in

255 the simulation with the estimated density. High accuracy is indicated by the mean

256 difference between the estimated and actual values not being significantly differ-

257 ent from zero (Wilcoxon signed-rank test). gREM precision was determined by

258 the standard deviation of estimated densities. We used this method to compare

259 the accuracy and precision of all the gREM submodels. As these submodels are

260 derived for different combinations of α and θ, the accuracy and precision of the

261 submodels was used to determine the impact of different values of α and θ.

262 The influence of the number of captures and animal movement models on ac-

263 curacy and precision was investigated using four different gREM submodels rep-

264 resentative of the range α and θ values (submodels NW1, SW1, NE1, and SE3,

265 Figure 2). Using these four submodels, we calculated how long the simulation

266 needed to run to generate a range of different capture numbers (from 10 to 100 cap-

267 tures in 10 unit intervals), and estimated animal density. These estimated densities

268 were compared to the real density to assess the impact on the accuracy and preci-

269 sion of the gREM. We calculated the coefficient of variation in order the compare

270 the precision between capture numbers. The gREM also assumes that individuals

271 move continuously with straight-line movement (simple movement model) and

272 we therefore assessed the impact of breaking the gREM assumptions. We used

273 the four submodels to compare the accuracy and precision of a simple movement

274 model, stop-start movement models (using different amounts of time spent sta-

275 tionary), and random walk movement models.

RESULTS

277 **Analytical model.** The equation for $\bar{p}$ has been newly derived for each submodel

278 in the gREM, except for the gas model and REM which have been calculated pre-

279 viously. However, many models, although derived separately, have the same ex-

280 pression for $\bar{p}$. Figure 4 shows the expression for $\bar{p}$ in each case. The general equa-

281 tion for density, using the correct expression for $\bar{p}$ is then substituted into eqn 3.

282 Although more thorough checks are performed in Appendix S3, it can be seen that

283 all adjacent expressions in Figure 4 are equal when expressions for the boundaries

284 between them are substituted in.

285 **Simulation model.**

286 *gREM submodels.* All gREM submodels showed a high accuracy, i.e., the mean

287 difference between the estimated and actual values was not significantly differ-

288 ent from zero across all models, corrected for multiple tests (all gREM sub models

289 Wilcoxon signed-rank test, p >0.002) (Figure 5). However, the precision of the sub-

290 models do vary, where the gas model is the most precise and the SW7 sub model

291 the least precise, having the smallest and the largest interquartile range, respec-

292 tively (Figure 5). The standard deviation of the error between the estimated and

293 true densities is strongly related to both the sensor and signal widths (Figure 6),

294 such that larger widths have lower standard deviations (greater precision).

295 *Number of captures.* Within the four gREM submodels tested (NW1, SW1, SE3,

296 NE1), the accuracy was not affected by the number of captures, where the mean

297 difference between the estimated and actual values was not significantly differ-

298 ent from zero across all capture rates, corrected for multiple tests (all gREM sub

299 models Wilcoxon signed-rank test, p >0.008) (Figure **??**). However, the precision

300 was dependent on the number of captures across all four of the gREM submod-

301 els, where precision increases as number of captures increases (Figure **??**). For all

302 gREM submodels, the the coefficient of variation falls to 10% at 100 captures.

303 *Movement models.* Within the four gREM submodels tested (NW1, SW1, SE3, NE1),

304 neither the accuracy or precision was affected by the amount of time spent sta-

305 tionary. The mean difference between the estimated and actual values was not

306 significantly different from zero for each category of stationary time (0, 0.25, 0.5

307 and 0.75), corrected for multiple tests (all gREM sub models Wilcoxon signed-rank

308 test, p >0.12) (Figure **??**). Altering the maximum change in direction in each step

309 (0, pi/3, 2pi/3, and pi) did not affect the accuracy or precision of the four gREM

310 submodels tested (all gREM sub models Wilcoxon signed-rank test, p >0.05) (Fig-

311 ure **??**).

312   DISCUSSION

313   We have developed the gREM such that it can be used to estimate density from

314 acoustic sensors and camera traps. This has entailed a generalisation of the gas

315 model and the REM in Rowcliffe *et al.* (2008) to be applicable to any combination

316 of sensor width and signal directionality. We have used simulations to show, as a

317 proof of principle, that these models are accurate and precise. The precision of the

318 gREM was found to be dependent on the width of the sensor and the signal, and

319 the number of captures.

320 **Analytical model.** The gREM was derived for different combinations of α and

321 θ resulting in 25 different submodels, the expression for $\bar{p}$ are equal for many of

322 these submodels resulting in eight different equations including the previously de-

323 rived gas model and REM. These submodels were tested for consistency with adja-

324 cent expressions being equal at their boundaries. These new submodels will allow

325 researchers to evaluate the absolute density of animals that have previously been

326 difficult to study, such as bats (Clement & Castleberry, 2013), with non-invasive

327 methods such as remote sensors. The gREM also allows the data from acoustic de-

328 tectors to be used where an animal has a directional calls, this could be used for a

329 range of animals including songbirds (Blumstein *et al.*, 2011), dolphins (Lammers

330 & Au, 2003), as well as bats (Adams *et al.*, 2013).

331   There are a number of possible extensions to the gREM which could be devel-

332 oped in the future. The original gas model was formulated for the case where both

333 subjects, either animal and detector, or animal and animal, are moving (Hutchin-

334 son & Waser, 2007). Indeed any of the models with animals that are equally de-

335 tectable in all directions ($\alpha = 2\pi$) can be trivially expanded for moving by substi-

336 tuting the sum of the average animal velocity and the sensor velocity for *v* as used

here. However, when the animal has a directional call, as seen in both terrestrial and aquatic environments (Lammers & Au, 2003; Blumstein *et al.*, 2011), the extension becomes less simple. The approach would be to calculate again the mean profile width. However, for each angle of approach, one would have to average the profile width for an animal facing in any direction (i.e. not necessarily moving towards the sensor) weighted by the relative velocity of that direction. There are a number of situations where a moving detector and animal could occur, e.g. an acoustic detector towed from a boat when studying porpoises (Kimura *et al.*, 2014) or surveying bats from a moving car (Ahlen & Baagøe, 1999; Jones *et al.*, 2013).

Interesting but unstudied problems impacting the gREM are firstly, edge effects caused by sensor trigger delays (the delay between sensing an animal and attempting to record the encounter) (Rovero *et al.*, 2013), and secondly, sensors which repeatedly turn on an off during sampling (Jones *et al.*, 2013). The second problem is particualrly relevant to acoustic detectors which record ultrasound by time expansion. Here ultrasound is recorded for a set time period and then slowed down and played back, rendering the sensor 'deaf' periodically during sampling. Both of these problems may cause biases in the gREM, as animals can move through the detection zone without being detected. As the gREm assumes constant surveillance, the error created by switching the sensor on and off quickly will become more important if the sensor is only on for short periods of time. For example, if it takes longer for the recording device to be switched on than the length of some animal calls then there could be a systematic underestimation of density. We recommend that the gREM is applied to constantly sampled data, and the impacts of breaking these assumptions on the gREM should be further explored.

Accuracy, Precision and Recommodations for Best Practice. Based on our simulations we believe that the gREM has the potential to produce accurate estimates for many different species, using either camera traps or acoustic detectors. However the precision of the gREM differed between submodels. For example, when the sensor and signal width were small, the precision of the model was reduced. Therefore when choosing a sensor for use in a gREM study, the sensor detection

width should be maximised. If the study species has a narrow signal direction-
ality, other aspects of the study protocol, such as length of the survey, should be
used to compensate.

The precision of the gREM is greatly affected by the number of captures. The
coefficient of variation falls dramatically between 10 and 60 captures and then
after this continues to slowly reduce. At 100 captures the submodels reach 10%
coefficient of variation, considered to a very good level of precision (Thomas &
Marques, 2012). Many current studies do not reach this level of precision, with
most studies reporting coefficient of variations greater than the 10% level (O'Brien
et al., 2003; Proctor *et al.*, 2010; Foster & Harmsen, 2012). The length of surveys
in the field will need to be adjusted so that enough data can be collected to reach
this precision level. Populations of fast moving animals or populations with high
densities will require less survey effort than those species that are slow moving or
have populations with low densities.

The gREM was both accurate and precise for all the movement models we
tested (stop-start movement and correlated random walks). However these move-
ment models are still simple representations of true animal movement which are
dependent on multiple factors such as behavioural state and existence of home
ranges (Smouse *et al.*, 2010). The accuracy of the gREM may be affected by the
interaction between the movement model and the size of the detection radius. We
have studied a relatively long step length compared to the size of the detection ra-
dius, and therefore the chance of catching the same animal multiple times within
a short space of time was reduced and there is little effect on the precision of the
model (Figure **??**). However if the ratio of step length to detection radius was
smaller then this may decrease the precision of the model, however this should
not decrease its accuracy.

Limitations. Although we have used simulations to validate the gREM submod-
els, much more robust testing is needed. Although difficult, proper field test val-
idation would be required before the models could be fully trusted. The REM
(Rowcliffe *et al.*, 2008) has already been field tested, and both Rowcliffe *et al.* (2008)

and Zero *et al.* (2013) both found that the REM was an effective manner of estimating animal densities (Rowcliffe *et al.*, 2008; Zero *et al.*, 2013). In some taxa gold standard methods of estimating animal density exist, such as capture mark recapture (Sollmann *et al.*, 2013). Where these gold standard exist or true numbers are known, a simultaneous gREM study could be completed to test the accuracy under field conditions, similar to the tests in Rowcliffe *et al.* (2008). An easier way to continue to evaluate the models is to run more extensive simulations which break the assumptions of the analytical models. The main element that cannot be analytically treated is the complex movement of real animals. Therefore testing these methods against true animal traces, or more complex movement models would be required.

Within the simulation we have assumed an equal density across the entire world, however in a field environment the situation would be much more complex, with additional variation coming from local changes in density between sensor sites. We allowed the sensor to be stationary and continuously detecting, negating the triggering, and non-continuous recording issues that could exist with some sensors. In the simulation, the distance travelled of animal was assumed to be $40\,\mathrm{km\,day}^{-1}$, the largest day range of terrestrial animals (Carbone *et al.*, 2005). Other speed values should not alter the accuracy of the gREM, however, precision would be affected, all else being equal, since slower speeds produce fewer records. We also assume perfect knowledge of the average speed of an animal and size of the detection zone. All of which may lead to possible bias or a decrease in precision.

Implications for ecology and conservation. The gREM can estimate densities of a number of taxa where no, or few, accurate methods currently exist to measure absolute animal density and trends in absolute abundances (Thomas & Marques, 2012). Many of these species are critically endangered and monitoring their populations is of conservation interest. For example, current methods of density estimation for the threatened Francisana dolphin (*Pontoporia blainvillei*) may result in underestimation of their numbers (Crespo *et al.*, 2010). Our method may also be important for understanding zoonotic diseases, for example estimating population sizes of echolocating bats, which are important reservoir of infectious disease

15

that affect humans, livestock and wildlife (Calisher *et al.*, 2006). In addition, the gREM will make it possible to measure the density of animals which may be useful in quantifying ecosystem services, such as studying the levels of songbirds which are known to have a positive influence on pest control in coffee production (Jirinec *et al.*, 2011). The gREM is suitable for any species that would be consistently recorded within range of a detector, such as echolocating bats (Kunz *et al.*, 2009), songbirds (Buckland & Handel, 2006), whales (Marques *et al.*, 2009) or forest primates (Hassel-Finnegan *et al.*, 2008). With increasing technological capabilities, this list of species is likely to increase dramatically. Finally, the passive sensor methods that the gREM use are noninvasive and do not require individual marking (Jewell, 2013) or naturally identifying marks (as required for mark-recapture models). This makes them suitable for large, continuous monitoring projects with limited human resources (Kelly *et al.*, 2012). It also makes them suitable for species that are under pressure, species that cannot naturally be individually recognised or species that are difficult or dangerous to catch (Thomas & Marques, 2012).

1. ACKNOWLEDGMENTS

REFERENCES

Acevedo, M.A. & Villanueva-Rivera, L.J. (2006) Using automated digital recording systems as effective tools for the monitoring of birds and amphibians. *Wildlife Society Bulletin*, **34**, 211–214.

Adams, R.A., Pedersen, S.C., Walters, C., Collen, A., Lucas, T., Mroz, K., Sayer, C. & Jones, K. (2013) *Challenges of Using Bioacoustics to Globally Monitor Bats*, pp. 479–499. Springer New York.

Ahlen, I. & Baagøe, H.J. (1999) Use of ultrasound detectors for bat studies in europe: experiences from field identification, surveys, and monitoring. *Acta Chiropterologica*, **1**, 137–150.

Anderson, D.R. (2001) The need to get the basics right in wildlife field studies. *Wildlife Society Bulletin*, **29**, 1294–1297.

Barlow, J. & Taylor, B. (2005) Estimates of sperm whale abundance in the northeastern temperate pacific from a combined acoustic and visual survey. *Marine Mammal Science*, **21**, 429–445.

Blumstein, D.T., Mennill, D.J., Clemins, P., Girod, L., Yao, K., Patricelli, G., Deppe, J.L., Krakauer, A.H., Clark, C., Cortopassi, K.A. *et al.* (2011) Acoustic monitoring in terrestrial environments using microphone arrays: applications, technological considerations and prospectus. *Journal of Applied Ecology*, **48**, 758–767.

Borchers, D., Distiller, G., Foster, R., Harmsen, B. & Milazzo, L. (2014) Continuous-time spatially explicit capture–recapture models, with an application to a jaguar camera-trap survey. *Methods in Ecology and Evolution*, **5**, 656–665.

Brusa, A. & Bunker, D.E. (2014) Increasing the precision of canopy closure estimates from hemispherical photography: Blue channel analysis and under-exposure. *Agricultural and Forest Meteorology*, **195**, 102–107.

Buckland, S.T. & Handel, C. (2006) Point-transect surveys for songbirds: robust methodologies. *The Auk*, **123**, 345–357.

Buckland, S.T., Marsden, S.J. & Green, R.E. (2008) Estimating bird abundance: making methods work. *Bird Conservation International*, **18**, S91–S108.

Calisher, C., Childs, J., Field, H., Holmes, K. & Schountz, T. (2006) Bats: important reservoir hosts of emerging viruses. *Clinical Microbiology Reviews*, **19**, 531–545.

Carbone, C., Cowlishaw, G., Isaac, N.J. & Rowcliffe, J.M. (2005) How far do animals go? Determinants of day range in mammals. *The American Naturalist*, **165**, 290–297.

Clark, C.W. (1995) Application of US Navy underwater hydrophone arrays for scientific research on whales. *Reports of the International Whaling Commission*, **45**, 210–212.

Clement, M.J. & Castleberry, S.B. (2013) Estimating density of a forest-dwelling bat: a predictive model for rafinesque's big-eared bat. *Population Ecology*, **55**,

205–215.

Crespo, E.A., Pedraza, S.N., Grandi, M.F., Dans, S.L. & Garaffo, G.V. (2010) Abundance and distribution of endangered franciscana dolphins in argentine waters and conservation implications. *Marine Mammal Science*, **26**, 17–35.

Cutler, T.L. & Swann, D.E. (1999) Using remote photography in wildlife ecology: a review. *Wildlife Society Bulletin*, **27**, 571–581.

Damuth, J. (1981) Population density and body size in mammals. *Nature*, **290**, 699–700.

Depraetere, M., Pavoine, S., Jiguet, F., Gasc, A., Duvail, S. & Sueur, J. (2012) Monitoring animal diversity using acoustic indices: implementation in a temperate woodland. *Ecological Indicators*, **13**, 46–54.

Elphick, C.S. (2008) How you count counts: the importance of methods research in applied ecology. *Journal of Applied Ecology*, **45**, 1313–1320.

Everatt, K.T., Andresen, L. & Somers, M.J. (2014) Trophic scaling and occupancy analysis reveals a lion population limited by top-down anthropogenic pressure in the limpopo national park, mozambique. *PloS one*, **9**, e99389.

Foster, R.J. & Harmsen, B.J. (2012) A critique of density estimation from camera-trap data. *The Journal of Wildlife Management*, **76**, 224–236.

Harris, D., Matias, L., Thomas, L., Harwood, J. & Geissler, W.H. (2013) Applying distance sampling to fin whale calls recorded by single seismic instruments in the northeast atlantic. *The Journal of the Acoustical Society of America*, **134**, 3522–3535.

Hassel-Finnegan, H.M., Borries, C., Larney, E., Umponjan, M. & Koenig, A. (2008) How reliable are density estimates for diurnal primates? *International Journal of Primatology*, **29**, 1175–1187.

Hayes, J.P. (2000) Assumptions and practical considerations in the design and interpretation of echolocation-monitoring studies. *Acta Chiropterologica*, **2**, 225–236.

Hutchinson, J.M.C. & Waser, P.M. (2007) Use, misuse and extensions of "ideal gas" models of animal encounter. *Biological Reviews of the Cambridge Philosophical Society*, **82**, 335–359.

Jewell, Z. (2013) Effect of monitoring technique on quality of conservation science. *Conservation Biology*, **27**, 501–508.

Jirinec, V., Campos, B.R. & Johnson, M.D. (2011) Roosting behaviour of a migratory songbird on jamaican coffee farms: landscape composition may affect delivery of an ecosystem service. *Bird Conservation International*, **21**, 353–361.

Jones, K.E., Bielby, J., Cardillo, M., Fritz, S.A., O'Dell, J., Orme, C.D.L., Safi, K., Sechrest, W., Boakes, E.H., Carbone, C., Connolly, C., Cutts, M.J., Foster, J.K., Grenyer, R., Habib, M., Plaster, C.A., Price, S.A., Rigby, E.A., Rist, J., Teacher, A., Bininda-Emonds, O.R.P., Gittleman, J.L., Mace, G.M., Purvis, A. & Michener, W.K. (2009) Pantheria: a species-level database of life history, ecology, and geography of extant and recently extinct mammals. *Ecology*, **90**, 2648.

Jones, K.E., Russ, J.A., Bashta, A.T., Bilhari, Z., Catto, C., Csősz, I., Gorbachev, A., Győrfi, P., Hughes, A., Ivashkiv, I., Koryagina, N., Kurali, A., Langton, S., Collen, A., Margiean, G., Pandourski, I., Parsons, S., Prokofev, I., Szodoray-Paradi, A., Szodoray-Paradi, F., Tilova, E., Walters, C.L., Weatherill, A. & Zavarzin, O. (2013) *Indicator Bats Program: A System for the Global Acoustic Monitoring of Bats*, pp. 211–247. Wiley-Blackwell.

Karanth, K. (1995) Estimating tiger (*Panthera tigris*) populations from camera-trap data using capture–recapture models. *Biological Conservation*, **71**, 333–338.

Kelly, M.J., Betsch, J., Wultsch, C., Mesa, B. & Mills, L.S. (2012) Noninvasive sampling for carnivores. *Carnivore ecology and conservation: a handbook of techniques (L Boitani and RA Powell, eds) Oxford University Press, New York*, pp. 47–69.

Kessel, S., Cooke, S., Heupel, M., Hussey, N., Simpfendorfer, C., Vagle, S. & Fisk, A. (2014) A review of detection range testing in aquatic passive acoustic telemetry studies. *Reviews in Fish Biology and Fisheries*, **24**, 199–218.

Kimura, S., Akamatsu, T., Dong, L., Wang, K., Wang, D., Shibata, Y. & Arai, N. (2014) Acoustic capture-recapture method for towed acoustic surveys of echolocating porpoises. *The Journal of the Acoustical Society of America*, **135**, 3364–3370.

Kunz, T.H., Betke, M., Hristov, N.I. & Vonhof, M. (2009) Methods for assessing colony size, population size, and relative abundance of bats. *Ecological and behavioral methods for the study of bats (TH Kunz and S Parsons, eds) 2nd ed Johns Hopkins University Press, Baltimore, Maryland*, pp. 133–157.

Lammers, M.O. & Au, W.W. (2003) Directionality in the whistles of hawaiian spinner dolphins (stenella longirostris): A signal feature to cue direction of movement? *Marine Mammal Science*, **19**, 249–264.

Lewis, T., Gillespie, D., Lacey, C., Matthews, J., Danbolt, M., Leaper, R., McLanaghan, R. & Moscrop, A. (2007) Sperm whale abundance estimates from acoustic surveys of the ionian sea and straits of sicily in 2003. *Journal of the Marine Biological Association of the United Kingdom*, **87**, 353–357.

Manzo, E., Bartolommei, P., Rowcliffe, J.M. & Cozzolino, R. (2012) Estimation of population density of european pine marten in central italy using camera trapping. *Acta Theriologica*, **57**, 165–172.

Marcoux, M., Auger-Méthé, M., Chmelnitsky, E.G., Ferguson, S.H. & Humphries, M.M. (2011) Local passive acoustic monitoring of narwhal presence in the canadian arctic: a pilot project. *Arctic*, **64**, 307–316.

Marques, T.A., Munger, L., Thomas, L., Wiggins, S. & Hildebrand, J.A. (2011) Estimating North Pacific right whale (*Eubalaena japonica*) density using passive acoustic cue counting. *Endangered Species Research*, **13**, 163–172.

Marques, T.A., Thomas, L., Ward, J., DiMarzio, N. & Tyack, P.L. (2009) Estimating cetacean population density using fixed passive acoustic sensors: An example with Blainville's beaked whales. *The Journal of the Acoustical Society of America*, **125**, 1982–1994.

O'Brien, T.G., Kinnaird, M.F. & Wibisono, H.T. (2003) Crouching tigers, hidden prey: Sumatran tiger and prey populations in a tropical forest landscape. *Animal Conservation*, **6**, 131–139.

O'Farrell, M.J. & Gannon, W.L. (1999) A comparison of acoustic versus capture techniques for the inventory of bats. *Journal of Mammalogy*, **80**, 24–30.

Proctor, M., McLellan, B., Boulanger, J., Apps, C., Stenhouse, G., Paetkau, D. & Mowat, G. (2010) Ecological investigations of grizzly bears in canada using dna from hair, 1995-2005: a review of methods and progress. *Ursus*, **21**, 169–188.

Purvis, A., Gittleman, J.L., Cowlishaw, G. & Mace, G.M. (2000) Predicting extinction risk in declining species. *Proceedings of the Royal Society of London Series B: Biological Sciences*, **267**, 1947–1952.

Richter-Dyn, N. & Goel, N.S. (1972) On the extinction of a colonizing species. *Theoretical Population Biology*, **3**, 406–433.

Rogers, T.L., Ciaglia, M.B., Klinck, H. & Southwell, C. (2013) Density can be misleading for low-density species: benefits of passive acoustic monitoring. *Public Library of Science One*, **8**, e52542.

Rovero, F., Zimmermann, F., Berzi, D. & Meek, P. (2013) "Which camera trap type and how many do I need?" a review of camera features and study designs for a range of wildlife research applications. *Hystrix*, **24**, 148–156.

Rowcliffe, J.M. & Carbone, C. (2008) Surveys using camera traps: are we looking to a brighter future? *Animal Conservation*, **11**, 185–186.

Rowcliffe, J., Field, J., Turvey, S. & Carbone, C. (2008) Estimating animal density using camera traps without the need for individual recognition. *Journal of Applied Ecology*, **45**, 1228–1236.

Schmidt, B.R. (2003) Count data, detection probabilities, and the demography, dynamics, distribution, and decline of amphibians. *Comptes Rendus Biologies*, **326**, 119–124.

Smouse, P.E., Focardi, S., Moorcroft, P.R., Kie, J.G., Forester, J.D. & Morales, J.M. (2010) Stochastic modelling of animal movement. *Philosophical Transactions of the Royal Society B: Biological Sciences*, **365**, 2201–2211.

Soisalo, M.K. & Cavalcanti, S. (2006) Estimating the density of a jaguar population in the Brazilian Pantanal using camera-traps and capture-recapture sampling in combination with GPS radio-telemetry. *Biological Conservation*, **129**, 487–496.

Sollmann, R., Gardner, B., Chandler, R.B., Shindle, D.B., Onorato, D.P., Royle, J.A. & O'Connell, A.F. (2013) Using multiple data sources provides density estimates for endangered florida panther. *Journal of Applied Ecology*, **50**, 961–968.

SymPy Development Team (2014) *SymPy: Python library for symbolic mathematics*.

Team, R.C. (2014) *R: A Language and Environment for Statistical Computing*. R Foundation for Statistical Computing, Vienna, Austria.

Thomas, L. & Marques, T.A. (2012) Passive acoustic monitoring for estimating animal density. *Acoustics Today*, **8**, 35–44.

Trolle, M. & Kéry, M. (2003) Estimation of ocelot density in the Pantanal using capture-recapture analysis of camera-trapping data. *Journal of Mammalogy*, **84**,

607–614.

Trolle, M., Noss, A.J., Lima, E.D.S. & Dalponte, J.C. (2007) Camera-trap studies of maned wolf density in the Cerrado and the Pantanal of Brazil. *Biodiversity and Conservation*, **16**, 1197–1204.

Wright, S.J. & Hubbell, S.P. (1983) Stochastic extinction and reserve size: a focal species approach. *Oikos*, pp. 466–476.

Yapp, W. (1956) The theory of line transects. *Bird Study*, **3**, 93–104.

Zero, V.H., Sundaresan, S.R., O'Brien, T.G. & Kinnaird, M.F. (2013) Monitoring an endangered savannah ungulate, Grevy's zebra (*Equus grevyi*): choosing a method for estimating population densities. *Oryx*, **47**, 410–419.
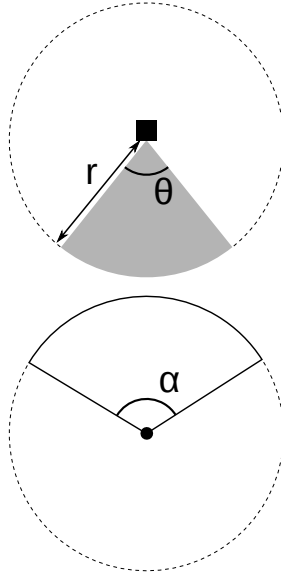
FIGURE 1. Representation of sensor detection width and animal signal width. The filled square and circle represent a sensor and an animal, respectively; θ, sensor detection width (radians); r, sensor detection distance; dark grey shaded area, sensor detection zone; α, animal signal width (radians). Dashed lines around the filled square and circle represents the maximum extent of θ and α, respectively.
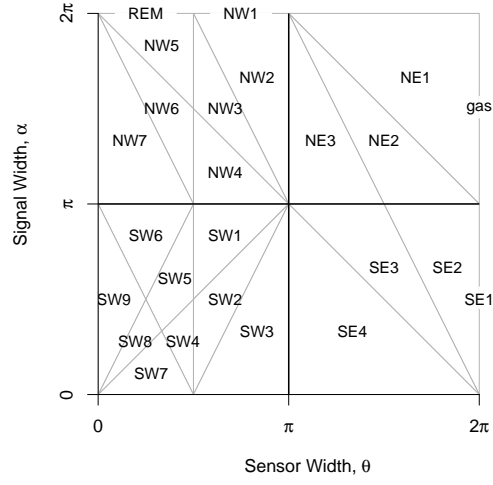
FIGURE 2. Locations where derivation of the average profile $\bar{p}$ is the same for different combinations of sensor detection and animal signal widths. Symbols within each polygon refer to each gREM submodel named after their compass point, except for Gas and REM which highlight the position of these previously derived models within the gREM. Symbols on the edge of the plot are for submodels where $\alpha, \theta = 2\pi$
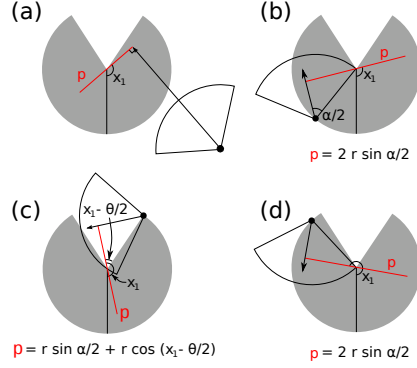
FIGURE 3. An overview of the derivation of the average profile $\bar{p}$ for the gREM submodel SE2, where (a) shows the location of the profile p (the line an animal must pass through in order to be captured) in red and the focal angle, x_1, for an animal (filled circle), its signal (unfilled sector), and direction of movement (shown as an arrow). The detection zone of the sensor is shown as a filled grey sector with a detection distance of r. The vertical black line within the circle shows the direction the sensor is facing. The derivation of p changes as the animal approaches the sensor from different directions (shown in b-d), where (b) is the derivation of p when x_1 is in the interval $[\frac{\pi}{2}, \frac{\pi}{2} + \frac{\theta}{2} - \frac{\alpha}{2}]$, (c) p when x_1 is in the interval $[\frac{\pi}{2} + \frac{\theta}{2} - \frac{\alpha}{2}, \frac{5\pi}{2} - \frac{\theta}{2} - \frac{\alpha}{2}]$ and (d) p when x_1 is in the interval $[\frac{5\pi}{2} - \frac{\theta}{2} - \frac{\alpha}{2}, \frac{3\pi}{2}]$, where θ, sensor detection width; α, animal signal width. The resultant equation for p is shown beneath b-d. The average profile $\bar{p}$ is the size of the profile averaged across all approach angles.
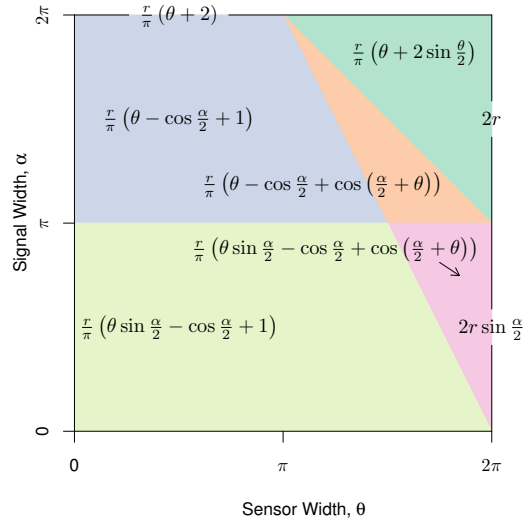
FIGURE 4. Expressions for the average profile width, $\bar{p}$, given a range of sensor and signal widths. Despite independent derivation within each block, many models result in the same expression. These are collected together and presented as one block of colour. Expressions on the edge of the plot are for submodels with $\alpha, \theta = 2\pi$.
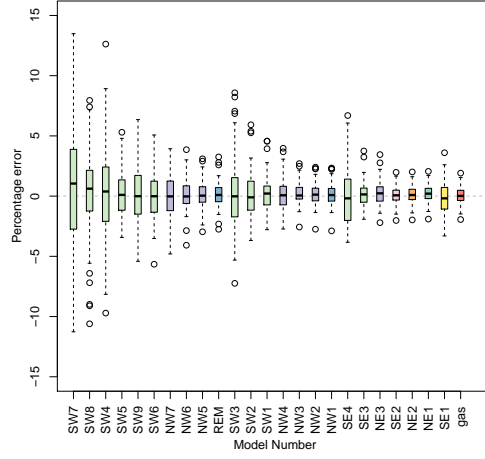
FIGURE 5. Simulation model results of the accuracy and precision for gREM submodels. The percentage error between estimated and true density for each gREM sub model is shown within each box plot, where the black line represents the median percentage error across all simulations, boxes represent the middle 50% of the data, whiskers represent variability outside the upper and lower quartiles with outliers plotted as individual points. Box colours correspond to the expressions for average profile width $\bar{p}$ given in Figure 4.
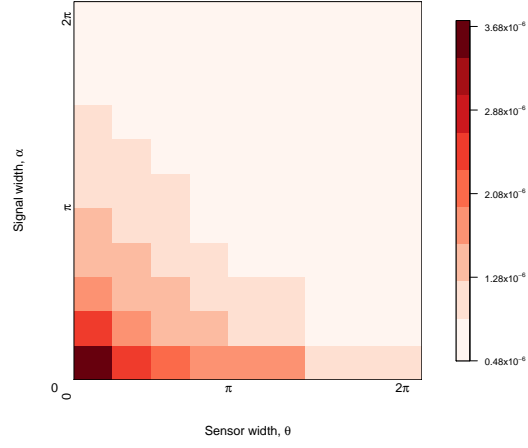
FIGURE 6. Simulation model results of the gREM precision given a range of sensor and signal widths, shown by the standard deviation of the error between the estimated and true densities. Standard deviations are shown from deep red to pink, representing high to low values between 0.483×10^{-6} to 3.74×10^{-6}.
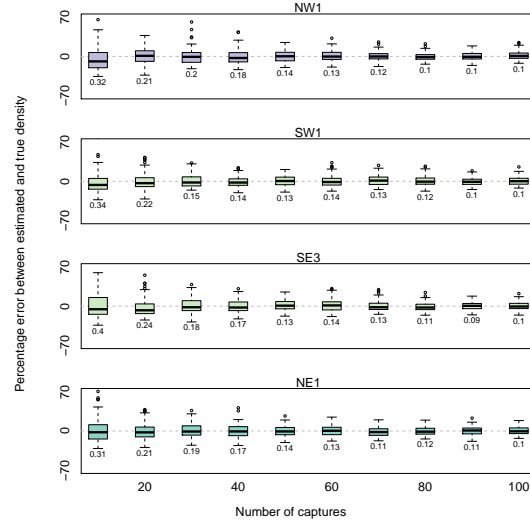
FIGURE 7. Simulation model results of the accuracy and precision of four gREM submodels (NW1, SW1, SE3 and NE1) given different numbers of captures. The percentage error between estimated and true density within each gREM sub model for capture rate is shown within each box plot, where the black line represents the median percentage error across all simulations, boxes represent the middle 50% of the data, whiskers represent variability outside the upper and lower quartiles with outliers plotted as individual points. Sensor and signal widths vary between submodels. The numbers beneath each plot represent the coefficient of variation. The colour of each box plot corresponds to the expressions for average profile width $\bar{p}$ given in Figure 4.
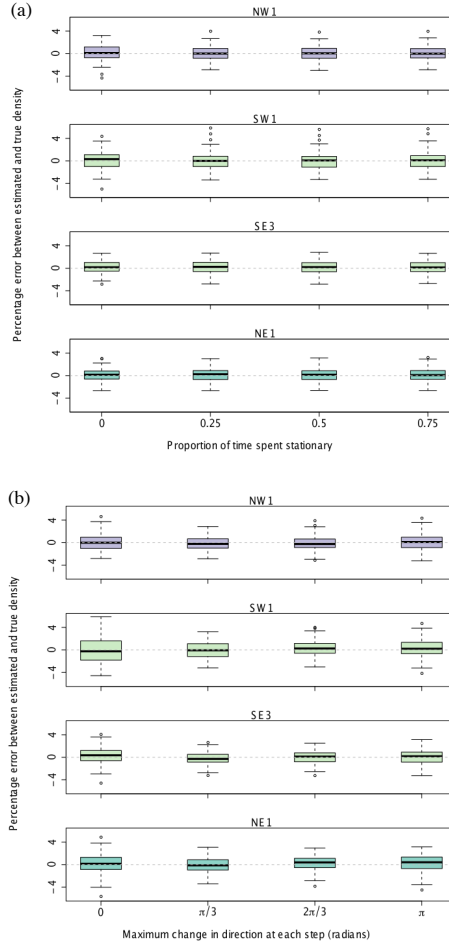
FIGURE 8. Simulation model results of the accuracy and precision of four gREM submodels (NW1, SW1, SE3 and NE1) given different movement models where (a) amount of time spent stationary (stop-start movement) and (b) maximum change in direction at each step (correlated random walk model). The percentage error between estimated and true density within each gREM sub model for the different movement models is shown within each box plot, where the black line represents the median percentage error across all simulations, boxes represent the middle 50% of the data, whiskers represent variability outside the upper and lower quartiles with outliers plotted as individual points. The simple model is represented where time and maximum change in direction equals 0. The colour of each box plot corresponds to the expressions for average profile width $\bar{p}$ given in Figure 4.